Dynamical simulation of neutron-induced fission of uranium isotopes using four-dimensional Langevin equations

M. R. Pahlavani* and S. M. Mirfathi

Department of Nuclear Physics, Faculty of Basic Science, University of Mazandaran, P.O. Box 47415-416, Babolsar, Iran

(Received 29 November 2015; revised manuscript received 16 February 2016; published 26 April 2016)

Four-dimensional Langevin equations have been suggested for the dynamical simulation of neutron-induced fission at low and medium excitation energies. The mass distribution of the fission fragments, the neutron multiplicity, and the fission cross section for the thermal and fast neutron-induced fission of ^{233}U, ^{235}U, and ^{238}U is studied by considering energy dissipation of the compound nucleus through the fission using four-dimensional Langevin equations combined with a Monte Carlo simulation approach. The calculated results using this approach indicate reasonable agreement with available experimental data.

DOI: 10.1103/PhysRevC.93.044617

I. INTRODUCTION

The mass distribution of the fission fragments and the multiplicity of γ rays and emitted neutrons are among the characteristics of neutron-induced fission in low excitation energies that have repeatedly come into focus as interesting features [1–7]. It is a well-known fact that the mass yield distribution in the neutron-induced fission of medium-Z actinides is asymmetric in nature [8]. Among the actinides, the fission of uranium isotopes is more interesting because of its application in accelerated driven subcritical system, conventional light and heavy water reactors, advanced heavy water reactors, and fast reactors [9–11]. Statistical descriptions of the fission process are often used to explain the experimental fission characteristics. By using the statistical scission-point model, the Weisskopf-type, or the Hauser-Feshbach approaches, the particle emission is simulated from the excited fission fragments based on sequential emission without considering time and the dynamical evolution of the fission process [12,13]. The transition state model (TSM) is one of the commonly used models developed to study the fission process. The fundamental assumptions of the TSM are that the spin projection (K) on the nuclear symmetry axis is conserved during the fission process and the transition time between the saddle and scission point is relatively short, so one can consider saddle or scission configuration as a compound nucleus characteristic.

The statistical scission-point model for fission, based on the assumption of statistical equilibrium among collective degrees of freedom at the scission point, allows the use of a parameter-free microcanonical statistical description to calculate the fission fragments' mass distribution and the mean values of all the fission observables [14–17]. These types of methods often define the shape of nuclear surface in a way that does not rely on any shape parametrization [18,19]. The statistical model is widely used to calculate the reaction rate as long as there is a sufficiently high density of excited states in the compound nuclei at the relevant bombarding energy, which occurs in the case of superheavy systems. However, at shell closures and by decreasing neutron energies, level densities at relevant compound formation energy in neutron-induced reactions become too small for such models to be practical [20]. Although equability of collective kinetic energies for constant distance between the tips of the fragments, and characterizing the excitation energy of the fragments with a nuclear temperature (independent of both the mass and the charge ratio) made the scission-point model an easily calculable approach [21], large amounts of experimental data indicate that the multiplicity of the prescission particles from excited nuclei exceeds the statistical model predictions. A correct understanding of the fission process requires a dynamical interpretation for evaluation of nucleons in excited compound nuclei. As it was suggested in the early 1950s, fission does not proceed only through one single pathway between the saddle and scission point. Also the statistical paths of the fission process could be explained more accurately by a proper Monte Carlo simulation scheme [22].

Due to importance of the incident neutron energy in the calculation of average prompt emitted quantities, which have provided important information about the effect of nuclear structure along with the dynamics of the descent from saddle to scission point [23,24], the present research is focused on the effects of the incident neutron energy on average multiplicity of prompt neutrons as well as the fission cross section. The rest of the present paper is organized as follows: The theoretical model is briefly described in Sec. II. Results of the present model with the available experimental data are compared in Sec. III. Finally a brief summary of the present study along with the concluding remarks are provided in Sec. IV.

II. DESCRIPTION OF THE MODEL

In the present study, the shape of a fissioning nuclei is restricted to the "funny hills" parametrization. The funny hills parameters c, h, and α respectively represent the elongation, the neck thickness, and the asymmetry. These parameters define the shape of the compound nucleus in cylindrical coordinates [25,26]:

$$\rho_s^2(z) = \begin{cases} (c^2 - z^2)\left(A_s + B_{sh}\,\frac{z^2}{c^2} + \alpha\,\frac{z}{c}\right) & \text{if } B_{sh} \geqslant 0, \\ (c^2 - z^2)\left(A_s + \alpha\,\frac{z}{c}\right)e^{(B_{sh}\,c\,z^2)} & \text{otherwise,} \end{cases} \quad (1)$$

*m.pahlavani@umz.ac.ir

where ρ_s is the radial coordinate of the compound nuclei, whose rotation about the symmetry axis determines the nuclear surface. z is the coordinate along the symmetry axis and c is the elongation parameter. $B_{sh} = 2h + (c-1)/2$ is the nuclear shape function. The quantity A_s, based on the conservation of nuclear volume, is defined as follows [26]:

$$A_s = \begin{cases} c^{-3} + B_{sh}/5 & \text{if } B_{sh} \geqslant 0, \\ -\frac{4}{3} \dfrac{B_{sh}}{\exp(B_{sh}\, c^3) + [1 + 1/(2\, B_{sh}\, c^3)]\sqrt{-\pi\, B_{sh}\, c^3}\ \mathrm{erf}(\sqrt{-B_{sh}\, c^3})} & \text{otherwise.} \end{cases} \tag{2}$$

The coupled four-dimensional Langevin equations are used in order to measure the evolution of the funny hills shape coordinates as [27]

$$\frac{dq_i}{dt} = \frac{p_j}{m_{ij}}, \tag{3}$$

$$\frac{dp_i}{dt} = -\frac{p_j\, p_k}{2} \frac{\partial}{\partial q_i}\left(\frac{1}{m_{jk}}\right) - \frac{\partial V}{\partial q_i} + T^2 \frac{\partial a}{\partial q_i} - \eta_{ij} \frac{dq_i}{dt} + R(t), \tag{4}$$

where $q_i = c$, h, and α, and $p_i = m_{ij} \frac{dq_j}{dt}$ is a momentum conjugate to coordinate q_i. As the compound nucleus is formed at a certain instant which is fixed as the origin of our dynamical calculation, the initial distribution of the coordinates and momenta are selected from sampling random numbers following the Maxwell-Boltzmann distribution [28–30]. Using the Monte Carlo method, the initial value of c in the interval (1.00,1.10) was sampled for each Langevin trajectory. m_{ij} is the inertia tensor, which is evaluated using the Werner-Wheeler formula [31,32],

$$m_{ij} = \pi\, \rho_m \int_{z_{\min}}^{z_{\max}} \rho_s^2(z)(A_i\, A_j + \rho_s^2(z)\, A_i'\, A_j'/8)\, dz, \tag{5}$$

where ρ_m is the mass density of the compound nucleus and $\bar{\upsilon}$ is the average speed of nucleons inside the nucleus. $z_{\min}$ and $z_{\max}$ are the left and the right boundaries of the compound nucleus surface, respectively. According to the Werner-Wheeler formula, A_i can be expressed as

$$A_i = -\frac{1}{\rho_s^2(z)} \frac{\partial}{\partial q_i} \int_{-c}^{z} \rho_s^2(z')\, dz'. \tag{6}$$

The quantity A' is the first derivative of A with respect to z. T is the temperature of the compound nucleus, which is related to its intrinsic energy through $T = \sqrt{E_{\mathrm{int}}/a}$. Also, E_{int} and a are, in order, the intrinsic energy of the system and the level density parameter, which will be defined in the following. In principle, the inertia and friction tensors may contain the shell effects. To account for these effects we need to consider the calculated microscopic transport coefficients, for example within the linear response theory and local harmonic approximation. But the calculated friction tensor in this approach is much smaller than those calculated by the macroscopic model at low temperature. The macroscopic friction and inertia tensors are used in the present paper. It should be mentioned here that the role of shell effects in the collective inertia and the friction coefficients is a physically complicated phenomenon and may require more information about the structure of the compound system. However, it would not affect the results of our calculations. The friction tensor in the wall-and-window one-body dissipation scheme for a small elongation before neck formation ($c < c_{\mathrm{win}}$) is given by [33]

$$\eta_{\mathrm{wall}_{ij}}(c < c_{\mathrm{win}}) = \frac{\pi\, \rho_m}{2}\, \overline{\upsilon} \int_{z_{\min}}^{z_{\max}} \left(\frac{\partial \rho_s^2}{\partial q_i}\right)\left(\frac{\partial \rho_s^2}{\partial q_j}\right)\left[\rho_s^2 + \left(\frac{1}{2}\frac{\partial \rho_s^2}{\partial z}\right)^2\right]^{-1/2} dz, \tag{7}$$

and, for an elongation greater than the point in which a neck is formed in the nuclear system ($c \geqslant c_{\mathrm{win}}$), the corresponding friction tensor can be written as [33]

$$\begin{aligned} \eta_{\mathrm{wall}_{ij}}(c \geqslant c_{\mathrm{win}}) = \frac{\pi\, \rho_m}{2}\, \overline{\upsilon} \Bigg\{ & \int_{z_{\min}}^{z_{\mathrm{neck}}} \left(\frac{\partial \rho_s^2}{\partial q_i} + \frac{\partial \rho_s^2}{\partial z}\frac{\partial D_1}{\partial q_i}\right)\left(\frac{\partial \rho_s^2}{\partial q_j} + \frac{\partial \rho_s^2}{\partial z}\frac{\partial D_1}{\partial q_j}\right)\left[\rho_s^2 + \left(\frac{1}{2}\frac{\partial \rho_s^2}{\partial z}\right)^2\right]^{-1/2} dz \\ & + \int_{z_{\mathrm{neck}}}^{z_{\max}} \left(\frac{\partial \rho_s^2}{\partial q_i} + \frac{\partial \rho_s^2}{\partial z}\frac{\partial D_2}{\partial q_i}\right)\left(\frac{\partial \rho_s^2}{\partial q_j} + \frac{\partial \rho_s^2}{\partial z}\frac{\partial D_2}{\partial q_j}\right)\left[\rho_s^2 + \left(\frac{1}{2}\frac{\partial \rho_s^2}{\partial z}\right)^2\right]^{-1/2} dz \Bigg\}, \end{aligned} \tag{8}$$

$$\eta_{\mathrm{win}_{ij}}(c \geqslant c_{\mathrm{win}}) = \frac{\pi\, \rho_m}{2}\, \overline{\upsilon}\left(\frac{\partial R}{\partial q_i}\frac{\partial R}{\partial q_j}\right)\Delta\sigma, \tag{9}$$

where $\bar{\upsilon} = \frac{3}{4}\upsilon$ is the average speed of nucleons inside the nucleus with υ as the Fermi velocity of the Fermi gas model. D_1 and D_2 represent the positions of the centers of two parts of a fissioning system, relative to the center of mass of the whole system. z_{neck} and $\Delta\sigma$ are the neck plane and the area of window between two parts of the system, respectively. Also,

R is the distance between the centers of mass of the nascent fragments. Eventually, after introducing a measure of chaos for the classical linear response theory regarding one-body dissipation, a scaled version of the friction (the chaos weighted wall and window friction) is obtained as [27,34]

$$\begin{aligned}\eta_{ij}(c < c_{\rm win}) &= \mu(c)\eta_{{\rm wall}_{ij}}(c < c_{\rm win}),\\ \eta_{ij}(c \geqslant c_{\rm win}) &= \mu(c)\eta_{{\rm wall}_{ij}}(c \geqslant c_{\rm win}) + \eta_{{\rm win}_{ij}}(c \geqslant c_{\rm win}).\end{aligned} \tag{10}$$

Here $\mu(c)$ is a measure of chaos that is varied randomly between 0 to 0.5 as the compound nucleus transforms from its initial spherical symmetric to a deformed shape. The normalized random force is assumed to be of the so-called white noise type, as presented in the relations

$$\langle R_i(t)\rangle = 0, \quad \langle R_i(t_1)R_j(t_2)\rangle = 2\delta_{ij}\delta(t_1 - t_2). \tag{11}$$

The evolution of the orientation degree of freedom (K coordinate) is obtained from the solution of the Langevin equations [26]

$$dK = -\frac{\gamma_K^2 I^2}{2}\frac{\partial V}{\partial K}dt + \gamma_K I R(t)\sqrt{\frac{T\,dt}{2}}, \tag{12}$$

where γ_K is the friction parameter which controls the coupling between the orientation degree of freedom (K) and the heat bath [26]:

$$\gamma_K = \frac{1}{R_N R\sqrt{2\pi^3 n_0}}\sqrt{\frac{J_\parallel J_{\rm eff} J_R}{J_\perp^3}}, \tag{13}$$

where R_N and n_0 are the neck radius and the bulk flux in standard nuclear matter ($n_0 = 0.0263$ MeV zs fm^{-4}), respectively. $J_\parallel$ and $J_\perp$ are, in order, the rigid body moments of inertia about and perpendicular to the symmetry axis, and $J_R = MR^2/4$ with M as the mass of compound nucleus. Also, $J_{\rm eff}^{-1} = J_\parallel^{-1} - J_\perp^{-1}$ is the effective moment of inertia. The initial value of K for each Langevin trajectory was generated from a uniform distribution (as a function of angular momentum L) using the Monte Carlo method in the interval $(-L,L)$ [35].

The modified potential energy of the system contains the liquid-drop, the rotational, and the microscopic parts, which are described below [23,35]:

$$\begin{aligned}V(q,I,K,T) = V_{LD}(q) &+ \frac{[I(I+1) - K^2]\hbar^2}{J_\perp(q)0.8MR_0^2 + 8Ma^2}\\ &+ \frac{K^2\hbar^2}{J_\parallel(q)0.8MR_0^2 + 8Ma^2} + V_{SH}(q,T).\end{aligned} \tag{14}$$

Here $V_{LD}(q)$ is the potential energy that is calculated based on the LDM, as a sum of the surface (E_S) and the Coulomb potential energy (E_C) [36]. The second and third terms on the right-hand side of Eq. (5) are the rotational energy. I and K are the total spin and its projection on symmetry axis, respectively. $R_0 = 1.2249A_{C.N.}^{1/3}$, with $A_{C.N.}$ as the mass number of the compound nucleus and $a = 0.6$ fm [35].

The moments of inertia ($J_\parallel$ and $J_\perp$) are obtained for a liquid-drop nucleus with a sharp boundary as a function of the distance between mass centers (q) in units of the corresponding spherical values. The temperature-dependent shell correction energy as a microscopic part of the potential energy is denoted by V_{SH} as

$$V_{SH}(q,T) = [\Delta E_{\rm pair}(q) + \Delta E_{\rm shell}(q)]\Phi(T), \tag{15}$$

where $\Delta E_{\rm pair}(q)$ is the pairing correlation energy in the BCS approximation [25,37]. Also, the shell correction energy based on the Strutinsky method is denoted by $\Delta E_{\rm shell}(q)$ as the difference between the sum of the single-particle energies of occupied states and the average density of single-particle states [16,25,38]:

$$\Delta E_{\rm shell}(q) = \sum_k \epsilon_k - \int_{-\infty}^{\mu} e g(e) de. \tag{16}$$

In the above relation, the energy, the chemical potential, and the parameter of density of states for the single-particle representation are presented by ϵ_k, μ, and $g(e)$, respectively. The temperature dependence part of the shell correction $\Phi(T)$ is [39]

$$\Phi(T) = \exp\left(-\frac{aT^2}{E_d}\right), \tag{17}$$

where E_d is the shell damping energy which is considered to be 25 MeV and a is the level density parameter that is evaluated as [40]

$$a = \left\{1 + \frac{V_{SH}(T=0)}{E_{\rm int}}\left[1 - \exp\left(-\frac{E_{\rm int}}{E_d}\right)\right]\right\}\tilde{a}(q), \tag{18}$$

where

$$\tilde{a}(q) = a_1 A_{C.N.} + a_2 A_{C.N.}^{2/3} B_s(q). \tag{19}$$

The volume and surface coefficients using LDM are $a_1 = 0.068$ and $a_2 = 0.213$, respectively. Also, $B_s(q)$ is the dimensionless function of the surface energy in the LDM with a sharp surface [25]. The intrinsic energy of system, ($E_{\rm int}$) is calculated at every step of the Langevin trajectory by the relation

$$E_{\rm int} = E_{C.M.} - Q - \frac{p_i\, p_j}{2\, m_{ij}} - V(q,l,T=0), \tag{20}$$

where $E_{C.M.}$ and Q are the energy of the system in the center-of-mass reference frame and the Q value of the reaction, respectively. In the present dynamical approach, each fission event is defined as the instance that the Langevin trajectory overcomes the scission point on the potential energy surface in which the configuration of the neck radius becomes zero. Shape evolution of the compound nuclei proceeds in competition with prescission particle emissions and fission. Multiplicity of prompt neutrons is simulated through Weisskopf's conventional evaporation theory under the following outlines. The neutron decay width is calculated using the relation [41,42]

$$\Gamma_n = \frac{2m_n}{[\pi\hbar]^2\rho_c(E_{\rm int})}\int_0^{E_{\rm int}-B_n}\rho_d(E_{\rm int} - \varepsilon_n)\varepsilon_n\sigma_{\rm inv}d\varepsilon_n, \tag{21}$$

where m_n is the reduced mass of the neutron with respect to the residual nucleus and B_n shows the binding energy of the compound nucleus. Also, ρ_c is the level density of the compound nuclei and ε_n is the average kinetic energy of the emitted

neutrons. Here $\sigma_{\rm inv}(\varepsilon_n) = \pi R_n^2$ is the inverse cross-section for the reaction $(A-1)+n \rightarrow A$, and R_n can be evaluated via $R_n = 1.21[(A-1)^{1/3}+1] + 3.4/\sqrt{\varepsilon_n}$. Calculation of the cross-section for the neutron-induced fission reaction, based on an extended statistical model, predicts a significant change in the properties of fission fragments [2,43]. Practically, distribution of a fragment's mass and fission cross section in the statistical model for neutron-induced fission reactions is obtained using a proper distribution function which depends on fission transition coefficients. In the present dynamical approach, a Monte Carlo algorithm is applied to calculate the competition between neutron emission and fission. Neutron decay width and the decay rate of fission, which depend upon the excitation energy, spin, and the mass number of each nuclei, have been evaluated in every evaluation time interval of the fissioning nucleus by employing the Langevin equations. To calculate the competition between neutron emission and fission by using the Monte Carlo technique, in the first step a random number r on the half-open interval [0,1) is selected. The random number is a numerical characteristic assigned to an element of the sample space. Then the probability of neutron emission is defined by $x = \tau/\tau_n$, where τ_n is the neutron decay time and τ is the time step of the calculation. If $r < x$, it will be interpreted as a particle emission, otherwise it will be clarified as fission, which determines the fission probability. The cross section of $U(n+f)$ is then evaluated as the product of the formation cross section of the compound nucleus (obtained from optical model considerations) and the fission probability.

Following the same procedure, the type of the emitted particle is decided by the Monte Carlo simulation based on the law of radioactive decay for the emitted particles. After each emission, the intrinsic excitation energy of residual mass and spin of the excited fragments are recalculated due to the energy that was released based on the one-particle emission. The kinetic energy of the emitted neutron has been sampled from the Watt spectrum [44,45]:

$$\frac{dN_{\rm pre}}{d\varepsilon_n} = \frac{\sqrt{\varepsilon_n}}{\Gamma(3/2)\sqrt{T_{\rm pre}^3}} \exp\left(-\varepsilon_n/T_{\rm pre}\right). \tag{22}$$

Here we consider $T_{\rm pre} = 1.10 \pm 0.05$ MeV. After emission of a neutron, the intrinsic excitation energy of the compound nuclei is recalculated and the process is continued. After every fission event, the mass numbers of conjugate fragments are calculated as well. The total kinetic energy, TKE, of the fission fragments is calculated to clarify the configuration of the compound nuclei at the scission point, which is defined with zero neck radius configuration. The TKE of fission fragments can be evaluated by applying

$$\mathrm{TKE} = V_{\rm Coul} + E_{\rm Kin}, \tag{23}$$

where $V_{\rm Coul}$ is the Coulomb repulsion energy between pointlike charged fragments,

$$V_{\rm Coul} = \frac{Z_1 Z_2 e^2}{D}, \tag{24}$$

where Z_1 and Z_2 are the charges of each fragment in units of e, and D is the distance between centers of mass of the left and right parts of the nucleus at the scission point. It should be recalled that, unlike the statistical model, the distance between centers of mass is not considered to be same as for the nascent fragments. The kinetic energy term, which is denoted by $E_{\rm Kin}$, can also be calculated at the scission point:

$$E_{\rm Kin} = \frac{p_i p_j}{2m_{ij}}. \tag{25}$$

However the main contribution to the TKE comes from $V_{\rm Coul}$ since the average of $E_{\rm Kin}$ over all fission events is much less than $V_{\rm Coul}$.

III. RESULTS

The fission fragment yields are calculated within this approach for selected reactions $n_{th} + {}^{233}$U, $n_{\rm th} + {}^{235}$U, and $n_{\rm fast} + {}^{238}$U, that are shown in Figs. 1–3. As can be seen, the theoretical results are close to available experimental data [2,46,47] and so the contributions of the mass-asymmetric fission events of uranium isotopes have been clarified. As shown in these figures, the heavy fragment's mass yields are almost similar for all considered reactions, and as expected, the most probable masses of the heavy fragments are $A_{\rm Heavy} \approx$ 135–140, while the position of the peak of the light fragment is different for various isotopes. But as a whole, the peak positions of the light fragment yields are in accordance with the expected tendency $A_{\rm Light} \approx A_{C.N.} - 140$.

Also, visible yield distinctions for the light fragments in the different isotopes are observed in the vicinity of their maxima. It is seen that, for two light isotopes of uranium(^{233}U and ^{235}U), the theoretical mass yield of light fragments is a little bit lower than experimental data, but in the case of heavy isotopes(^{238}U) the theoretical yield of both light and heavy fragments is greater than the experimental data. In general, the presence and the position of each mass-asymmetric peak are reproduced rather well, and the widths and strengths of the peaks of the calculated mass distributions do not differ

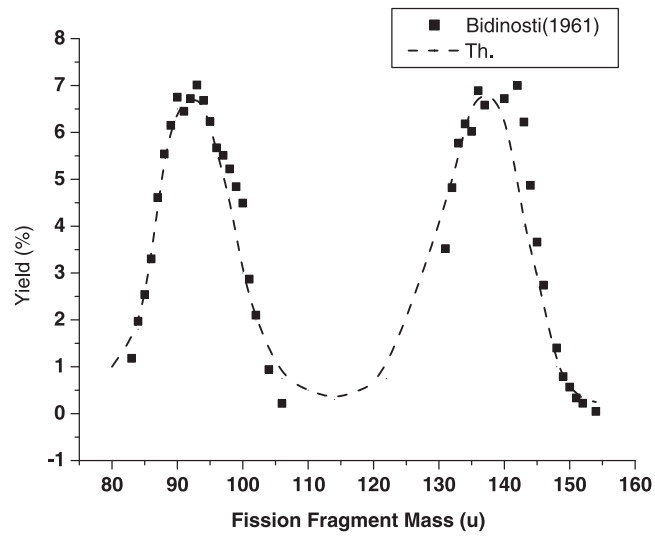

FIG. 1. Mass distribution of fragments in the thermal neutron-induced fission of ^{233}U. Experimental data [46] are denoted by the solid squares.

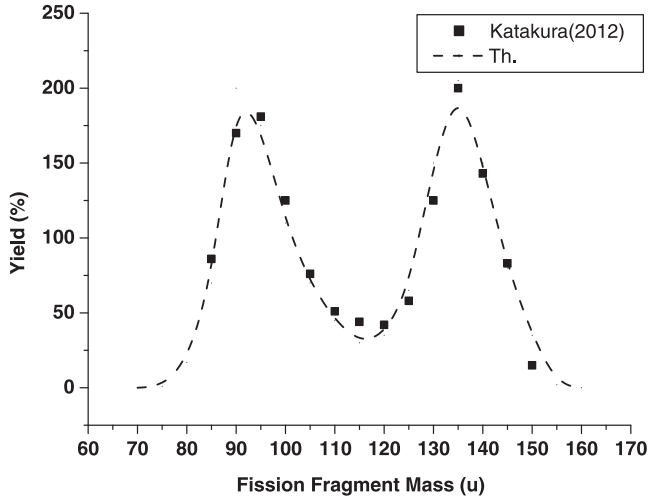

FIG. 2. Mass distribution of fragments in the thermal neutron-induced fission of ^{235}U. Experimental data [47] are denoted by the solid squares.

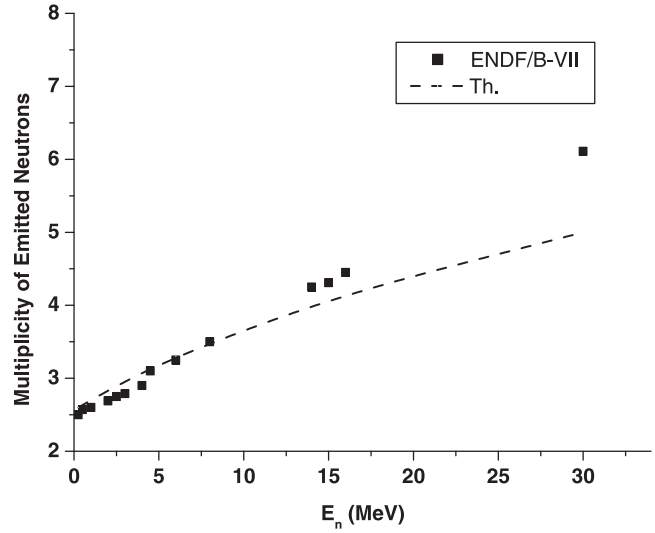

FIG. 4. Average multiplicity of emitted neutrons for ^{233}U as a function of incident neutron energy. Experimental data [48] are denoted by the solid squares.

substantially from the experimental data. There is only a minor shift from experimental data for heavier fragments. It should be noted that in the Langevin equations, the trajectories after overcoming the fission saddle point fluctuate frequently from the random force to reach this point. This approach enables us to determine the widths of fission fragment peaks. This feature may be the consequence of the remaining influence of excitation energy on the fragments' yield. Also, one can clearly see from Figs. 1–3 that the mass yields of the heavy fragments from different fissioning nuclei decrease with different slopes, especially in the case of $n_{\text{fast}} + {}^{238}$U, where the inclination of the mass distribution is smaller than in other isotopes. Such behavior of the fragments' yield indicates that the shapes of the asymmetric peaks are governed by shell closures formed in the heavy fragments, and by increasing incident neutron energy the influence of shell closures on the fragments' yield grows (especially for the light fragments). However, these asymmetric mass distributions are rather close to the experimental data. The presence and the position of each mass-asymmetric peak is reproduced rather well and the width and strength of the calculated mass distribution do not differ substantially from the experimental data.

Furthermore, the average multiplicities of prompt neutrons calculated as a function of incident neutron energies (E_n) in neutron-induced fission of ^{233}U, ^{235}U, and ^{238}U are shown in Figs. 4–6. At low incident neutron energies the agreement between results of the present model and the experimental data [48–50], which are denoted by solid squares, are satisfactory, but at high excitation energies such agreement is not achieved. Besides incident energies, the high average

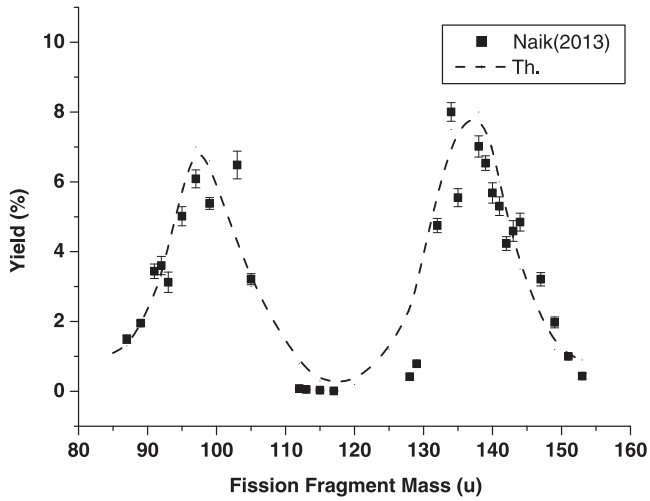

FIG. 3. Mass distribution of fragments in the fast neutron-induced fission of ^{238}U. Experimental data [2] are denoted by the solid squares.

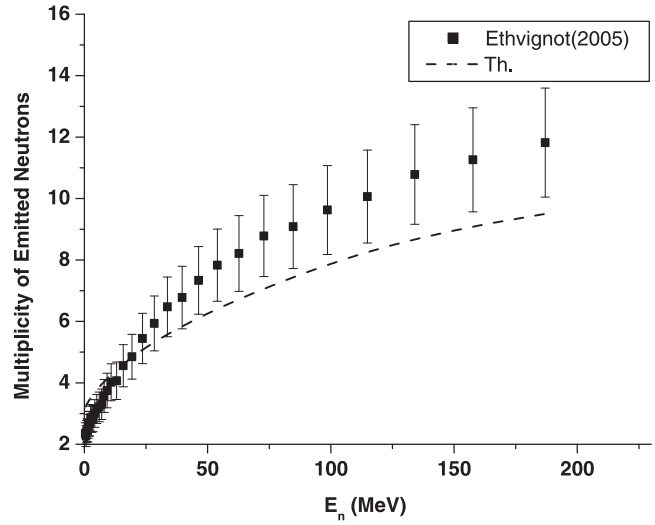

FIG. 5. Average multiplicity of emitted neutrons for ^{235}U as a function of the incident neutron energy. Experimental data [49] are denoted by the solid squares.

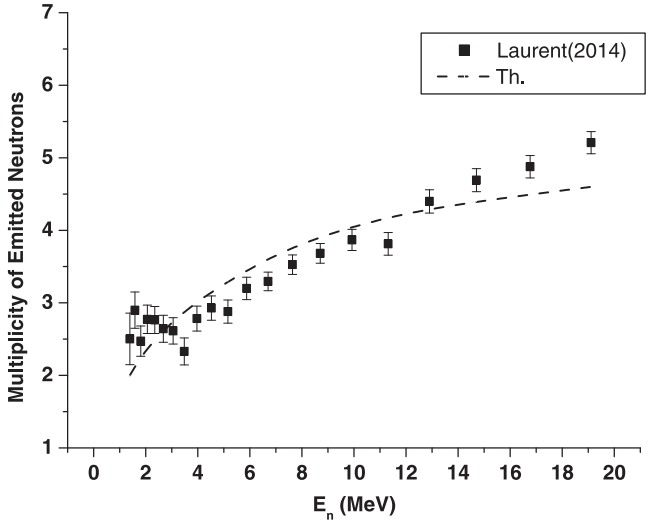

FIG. 6. Average multiplicity of emitted neutrons for ^{238}U as a function of the incident neutron energy. Experimental data [50] are denoted by the solid squares.

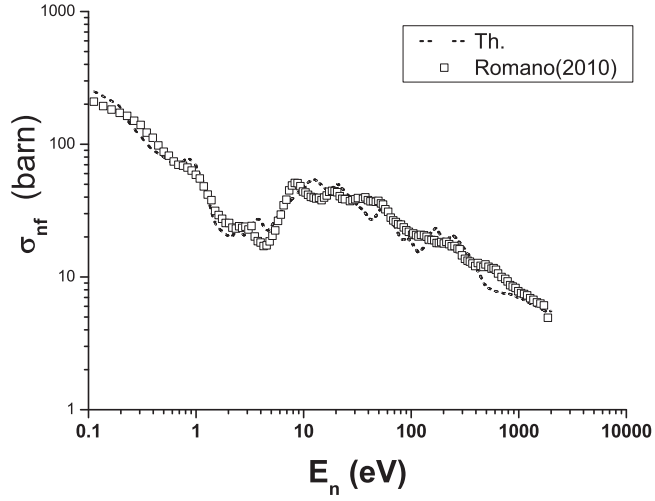

FIG. 8. Fission cross section for the reaction $n_{\rm th} + ^{235}$U as a function of the incident neutron energy. The theoretical results are denoted by the dashed line and the experimental data [52] are denoted by the open squares.

multiplicity of prompt neutron is due to the effect of the fissility parameter. Generally, with these theoretical considerations, the proportionality of neutron multiplicity versus incident neutron energies is consistent with the available experimental data. If we look at the trend of the theoretical neutron multiplicity, a decrement around energies higher than 10 MeV is observable. This deviation in comparison with the experimental data is not so surprising since the prompt neutron multiplicity mainly depends on the total excitation energy of each nucleus which is mainly related to incident neutron energies, and the parameters of the present approach (such as friction coefficient) which are developed for low-energy induced fission. Based on the earlier literature taking into account the fact that the multiplicity of prompt neutrons mainly depends on the fragments' TKE, similar little fluctuations of the total average multiplicity of neutrons are expected.

The fission cross section of $n_{\rm th} + ^{233}$U, $n_{\rm th} + ^{235}$U, and $n_{\rm fast} + ^{238}$U systems together with corresponding experimental data [51–53] are presented in Figs. 7–9. Analysis of the calculated fission cross sections in all selected reactions at low neutron energies show a good agreement with the experimental data, which confirms the validity of presented approach. However, at high excitation energies the calculated cross sections are lower than the experimental data. As is clear from these figures, a good agreement is achieved for ^{235}U and ^{238}U isotopes; nevertheless there is a shift in the cross section peaks between the theoretical results and the experimental data for higher energies in the fission of ^{233}U, but the uncertainty is satisfactory for such models. The smooth

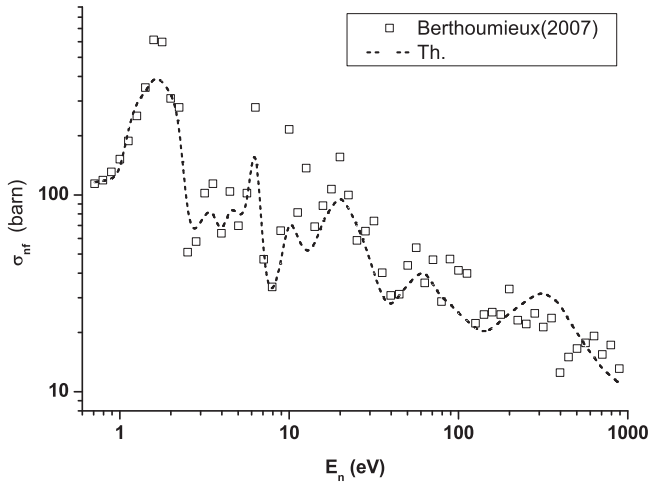

FIG. 7. Fission cross section for the reaction $n_{\rm th} + ^{233}$U as a function of the incident neutron energy. The theoretical results are denoted by the dashed line and the experimental data [51] are denoted by the open squares.

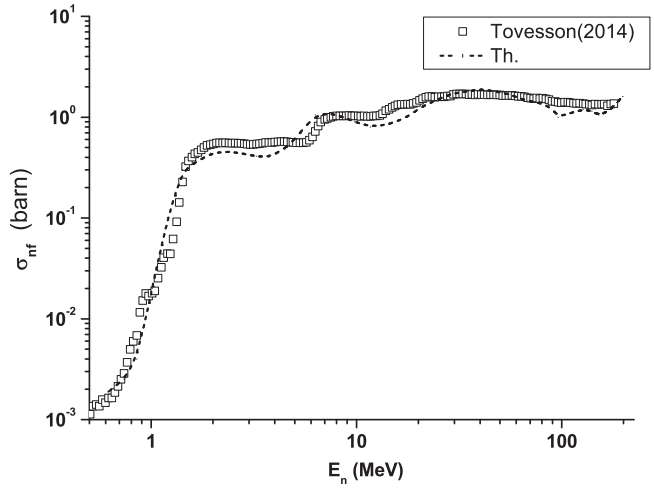

FIG. 9. Fission cross section for the reaction $n + ^{238}$U as a function of the incident neutron energy. The theoretical results are denoted by the dashed line and the experimental data [53] are denoted by the open squares.

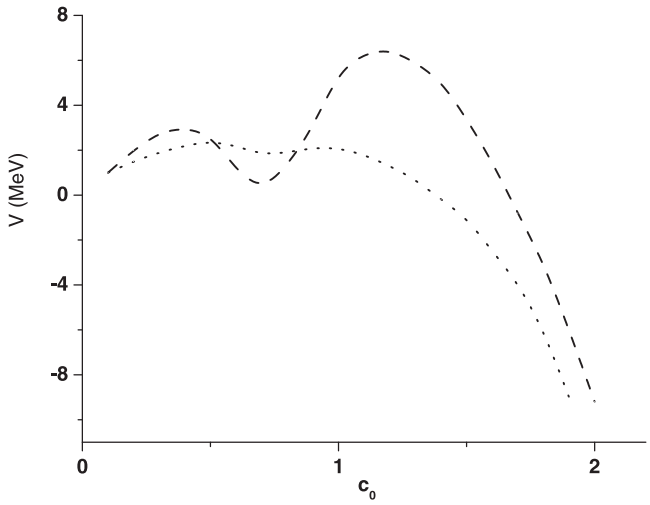

FIG. 10. Deformation dependence of the average potential energy for the reaction $n_{th} + {}^{235}U$ as a function of the distance between two potential centers. The asymmetric and symmetric cases are denoted by the dashed and dotted lines, respectively.

behavior of the fission cross sections down to thermal neutron energy, which also indicates the validity of the presente model, allowed a successful extrapolation of the fission cross section for the reaction ${}^{235}U(n_{th} + f)$ in energy range of eV, which led to an excellent agreement with the available experimental data obtained in the thermal energies region. In contrast to the reactions ${}^{235}U(n_{th} + f)$ and ${}^{238}U(n + f)$, the fission cross section for ${}^{233}U(n_{th} + f)$ has a more resonant structure for the subthreshold fission on a logarithmic scale. The calculated shape of the fission cross section for this reaction indicates large fluctuations, as shown in Fig. 7. It should be noted that there is some shape difference between the theoretical result and the experimental data, which is presumably due to the second-chance fission threshold energy being underestimated in this evaluation.

The average potential energy for ${}^{236}U$, which is formed in the $n_{th} + {}^{235}U$ reaction as a function of the distance between two potential centers, is presented in Fig. 10, with $\alpha \neq 0$ and $\alpha = 0$ indicated by the dashed and dotted lines, respectively. As shown in this figure, in the symmetric mode of fission for the $n_{th} + {}^{235}U$ reaction, with $\alpha = 0$ due to the neglecting microscopic effects, the potential energy decreases by a factor up to 2. One should remember that in the asymmetric mode the average potential energy is calculated over a wide range of α values for a large amount of fission events in the Langevin trajectories, and in this case α cannot be considered as a constant parameter.

TABLE I. The calculated and experimental average TKEs of the fission fragments. The theoretical results of the presented study are denoted by "Theor." and the experimental data [1,54,55] are indicated by "Expt."

Target	⟨TKE⟩ (MeV)		
	E_n	Theor.	Expt.
${}^{233}U$	0.025 (eV)	168.4	172.0 ± 1.8
${}^{235}U$	0.025 (eV)	169.3	168.2–171
${}^{238}U$	1.8 (MeV)	171.2	170.15 ± 0.07

The calculated average TKEs of the fission fragments are compared with available experimental data in Table I. The obtained results agree well with the experimental data. Due to this agreement, we conclude that the scission point configuration is compact.

IV. CONCLUSION

In the present study, the neutron-induced fission of three major isotopes of uranium was studied at different energies from thermal to fast, in terms of collective motion through the Langevin equations coupled with a Monte Carlo simulation to allow discrete emission of light particles and γ rays. Generally, the present dynamical Langevin mechanism along with Monte Carlo simulation was successful in reproducing the measured fission fragments' mass distribution, multiplicity of prompt neutrons, and fission cross section, especially for low neutron incident energies. Therefore, the present approach can serve as a basis for more refined analysis in different neutron-induced fissions.

ACKNOWLEDGMENTS

We would like to thank Mr. Pouya Pahlevani (University of Mysore, India), for his valuable suggestions and efforts during preparation of this paper, and also the University of Mazandaran (Iran) for financial support of this project.

[1] R. Vandenbosh and J. R. Huizenga, *Nuclear Fission* (Academic Press, New York, 1973).
[2] H. Naik, V. K. Mulik, P. M. Prajapati, B. S. Shivasankar, S. V. Suryanarayana, K. C. Jagadeesan, S. V. Thakare, S. C. Sharmae, and A. Goswami, Nucl. Phys. A **913**, 185 (2013).
[3] A. Tudora, F. J. Hambsch, G. Giubega, and I. Visan, Nucl. Phys. A **929**, 260 (2014).
[4] H. Goutte, J. F. Berger, P. Casoli, and D. Gogny, Phys. Rev. C **71**, 024316 (2005).
[5] S. Lemaire, P. Talou, T. Kawano, M. B. Chadwick, and D. G. Madland, Phys. Rev. C **73**, 014602 (2006).
[6] J. Randrup and R. Vogt, Phys. Rev. C **80**, 024601 (2009).
[7] P. Talou, B. Becker, T. Kawano, M. B. Chadwick, and Y. Danon, Phys. Rev. C **83**, 064612 (2011).
[8] C. Wagemans, *The Nuclear Fission Process* (CRC, London, 1990).
[9] S. Ganesan, Pramana J. Phys. A **68**, 257 (2007).
[10] R. K. Sinha and A. Kakodkar, Nucl. Eng. Des. **236**, 683 (2006).
[11] L. Mathieu *et al.*, in Proceedings of the 7th International Conference GLOBAL, Nuclear Energy Systems for Future Generation and Global Sustainability, Tsukuba, Japan, Paper No. 428, 2005 (unpublished).
[12] R. Vogt, J. Randrup, D. A. Brown, M. A. Descalle, and W. E. Ormand, Phys. Rev. C **85**, 024608 (2012).

[13] B. Becker, P. Talou, T. Kawano, Y. Danon, and I. Stetcu, Phys. Rev. C **87**, 014617 (2013).
[14] B. D. Wilkins, E. P. Steinberg, and R. R. Chasman, Phys. Rev. C **14**, 1832 (1976).
[15] J. F. Lemaitre, S. Panebianco, J. L. Sida, S. Hilaire, and S. Heinrich, Phys. Rev. C **92**, 034617 (2015).
[16] F. A. Ivanyuk, S. Chiba, and Y. Aritomo, Phys. Rev. C **90**, 054607 (2014).
[17] S. Goriely, S. Hilaire, A. J. Koning, and R. Capote, Phys. Rev. C **83**, 034601 (2011).
[18] V. M. Strutinsky, N. Ya. Lyashchenko, and N. A. Popov, Nucl. Phys. **46**, 639 (1963).
[19] F. A. Ivanyuk and K. Pomorski, Phys. Rev. C **79**, 054327 (2009).
[20] T. Rauscher, F.-K. Thielemann, and K.-L. Kratz, Phys. Rev. C **56**, 1613 (1997).
[21] J. Moreau, K. Heyde, and M. Waroquier, Phys. Rev. C **28**, 1640 (1983).
[22] S. M. Mirfathi and M. R. Pahlavani, Phys. Rev. C **78**, 064612 (2008).
[23] Y. Aritomo and S. Chiba, Phys. Rev. C **88**, 044614 (2013).
[24] Y. Aritomo, S. Chiba, and F. Ivanyuk, Phys. Rev. C **90**, 054609 (2014).
[25] M. Brack, J. Damgaard, A. S. Jensen, H. C. Pauli, V. M. Strutinsky, and C. Y. Wong, Rev. Mod. Phys. **44**, 320 (1972).
[26] P. N. Nadtochy, E. G. Ryabov, A. E. Gegechkori, Yu. A. Anischenko, and G. D. Adeev, Phys. Rev. C **85**, 064619 (2012).
[27] G. Chaudhuri and S. Pal, Phys. Rev. C **65**, 054612 (2002).
[28] P. Frobrich and I. I. Gontchar, Phys. Rep. **292**, 131 (1998).
[29] A. K. Dhara, K. Krishan, C. Bhattacharya, and S. Bhattacharya, Phys. Rev. C **57**, 2453 (1998).
[30] G. Chaudhuri and S. Pal, Phys. Rev. C **63**, 064603 (2001).
[31] H. Feldmeier, Rep. Prog. Phys. **50**, 915 (1987).
[32] K. T. R. Davies, A. J. Sierk, and J. R. Nix, Phys. Rev. C **13**, 2385 (1976).
[33] D. V. Vanin, G. I. Kosenko, and G. D. Adeev, Phys. Rev. C **59**, 2114 (1999).
[34] S. Pal and T. Mukhopadhyay, Phys. Rev. C **57**, 210 (1998).
[35] J. P. Lestone and S. G. McCalla, Phys. Rev. C **79**, 044611 (2009).
[36] A. J. Sierk, Phys. Rev. C **33**, 2039 (1986).
[37] S. G. Nilsson, C. F. Tsang, A. Sobiczewski, Z. Szymanski, S. Wycech, C. Gustafson, I. Lamm, P. Moller, and B. Nilsson, Nucl. Phys. A **131**, 1 (1969).
[38] V. M. Strutinsky, Nucl. Phys. A **95**, 420 (1967).
[39] T. Asano, T. Wada, M. Ohta, T. Ichikawa, S. Yamaji, and H. Nakahara, J. Nucl. Radiochem. Sci. **5**, 1 (2004).
[40] J. Toke and W. J. Swiatecki, Nucl. Phys. A **372**, 141 (1981).
[41] V. Weisskopf, Phys. Rev. **52**, 295 (1937).
[42] M. Blann, Phys. Rev. C **21**, 1770 (1980).
[43] E. Birgersson, A. Oberstedt, S. Oberstedt, and F.-J. Hambsch, Nucl. Phys. A **817**, 1 (2009).
[44] Y. Jia and J. D. Bao, Phys. Rev. C **75**, 034601 (2007).
[45] H. Rossner, D. J. Hinde, J. R. Leigh, J. P. Lestone, J. O. Newton, J. X. Wei, and S. Elfstrom, Phys. Rev. C **45**, 719 (1992).
[46] D. R. Bidinosti, D. E. Irish, and R. H. Tomlinson, Can. J. Chem. **39**, 628 (1961).
[47] K. Katakura, *JENDL FP Decay Data File 2011 and Fission Yields Data File 2011* (Japan Atomic Energy Agency, Tokai, 2012).
[48] http://www.nndc.bnl.org/endf/, Evaluated Nuclear Data File (ENDF), 2012.
[49] T. Ethvignot, M. Devlin, H. Duarte, T. Granier, R. C. Haight, B. Morillon, R. O. Nelson, J. M. O'Donnell, and D. Rochman, Phys. Rev. Lett **94**, 052701 (2005).
[50] B. Laurent, T. Granier, G. Bélier, A. Chatillon, J. F. Martin, J. Taieb, F. J. Hambsch, F. Tovesson, A. B. Laptev, R. C. Haight, R. O. Nelson, and J. M. O'Donnell, Nucl. Instrum. Methods Phys. Res., Sect. A **745**, 99 (2014).
[51] E. Berthoumieux *et al.*, in *The 2007 Conference on Nuclear Data for Science and Technology, Nice, 2007,* Vol. 1 (EDP Sciences, Les Ulis, France, 2007), p. 571.
[52] C. Romano, Y. Danon, R. Block, J. Thompson, E. Blain, and E. Bond, Phys. Rev. C **81**, 014607 (2010).
[53] F. Tovesson, A. Laptev, and T. S. Hill, Nucl. Sci. Eng. **178**, 57 (2014).
[54] F. Pleasonton, Phys. Rev. **174**, 1500 (1968).
[55] F. Vives, F. J. Hambsch, H. Bax, and S. Oberstedt, Nucl. Phys. A **662**, 63 (2000).